Mathematics and Computers in Simulation 252 (2027) 834–849

Contents lists available at ScienceDirect

Mathematics and Computers in Simulation

journal homepage: www.elsevier.com/locate/matcom

Original articles

A one-dimensional piecewise-smooth map with some economic applications

Serena Brianzoni [a], Giovanni Campisi [a,*], Alessio Frati [b], Carlo Lucheroni [c]

[a] Department of Management, Polytechnic University of Marche, Piazzale Martelli 8, 60121, Ancona, Italy
[b] Department of Mathematics and Physics, Catholic University of the Sacred Heart, Brescia, Italy
[c] School of Science and Technologies, University of Camerino, Via M. delle Carceri 9, 62032, Camerino, Italy

ARTICLE INFO

Keywords:
Piecewise-smooth maps
Border-collision bifurcations
Complex dynamics
Banking duopoly

ABSTRACT

We study the dynamics of a one-dimensional piecewise-smooth map consisting of two branches topologically related to the logistic function. This map is obtained by simplifying a recently proposed economic banking-duopoly framework; at the same time, it is mathematically interesting for its own right. The bifurcation structure of the economically meaningful regions of the parameter space of this dynamical map is analytically studied and detailed, especially focusing on border-collision bifurcations of its fixed points, and on the specific case where the fixed points are virtual. Numerical simulations are provided to support our analytic results.

1. Introduction

In recent years a significant number of books and papers have been published on the theoretical analysis of piecewise-smooth (PWS) dynamical maps, owing to their widespread use in dynamical systems applications. Many mathematical models rely on PWS systems, for example in physics and biology [1–3], as well as in economics and finance [4–11].

From a mathematical perspective, PWS maps are particularly interesting because they allow for border-collision bifurcations (BCBs). Specifically, PWS maps consist of distinct regions in which the dynamical equations differ from one region to another. These regions are separated by boundaries, *i.e.*, points where the map is non-smooth. BCBs occur when an invariant set of the map (such as a fixed point or a periodic orbit) approaches and collides with one of these boundaries as a parameter varies. When this collision is parametrically attained, it may lead to a drastic change in the supported dynamics, for instance, inducing a direct transition from regular to chaotic behavior or even causing trajectories to diverge [12–15]. Consequently, the BCB mechanism supported by PWS systems is of particular interest in applied dynamical studies, especially in fields such as economics and finance, where the analysis of stability and efficiency plays a central role. Accordingly, the study of BCBs in PWS frameworks has been applied to banking system modeling and macroprudential policy analysis, contexts in which regulatory rules frequently introduce thresholds and regime switches.

In mathematical economics, an initial strand of the literature related to banking system studies models of loan competition within discrete–time duopoly frameworks with boundedly rational adjustment. These contributions show how capital regulation policies may interact with the strategic behavior of participating agents, thereby generating endogenous cycles, multistability, and chaotic dynamics in credit quantities [6,7,9]. More recently, dynamic banking oligopoly models have been extended to explicitly incorporate additional balance-sheet frictions and expectation feedback mechanisms, confirming that nonlinear adjustment processes can render lending stability highly sensitive to structural and regulatory parameters [16]. Similarly, nonlinear phenomena emerge when credit

* Corresponding author.
E-mail address: g.campisi@univpm.it (G. Campisi).

https://doi.org/10.1016/j.matcom.2026.10.023
Received 7 March 2026; Received in revised form 20 September 2026; Accepted 13 October 2026
Available online 19 October 2026
0378-4754/© 2026 The Authors. Published by Elsevier B.V. on behalf of International Association for Mathematics and Computers in Simulation (IMACS). This is an open access article under the CC BY license (http://creativecommons.org/licenses/by/4.0/).

risk is introduced into bounded rationality models of bank competition, further highlighting the relevance of dynamical systems tools for the modeling and analysis of banking stability [17].

A second strand of the literature, related to macroprudential policy research, investigates the effects of reserve requirement limits — interpreted as boundaries — on loan-to-deposit ratios (LDRs), as well as the associated macroprudential corridors designed to mitigate liquidity risk and restrain credit booms. Empirical and institutional analyses clarify how LDR thresholds operate in practice and why they may induce discontinuous policy responses [18]. From a dynamical perspective, PWS modeling shows that LDR-based instruments can trigger BCBs and abrupt regime shifts in lending dynamics, particularly when the banking sector adjusts loan supply through profit-based gradient mechanisms [16,19]. However, existing contributions typically focus on selected parameter regions or rely predominantly on numerical exploration, thereby leaving open a research gap concerning a complete analytical partition of the parameter space into economically interpretable dynamical regimes.

To mention further contributions, discrete-time dynamical approaches have also been employed at the macroeconomic level to model the intermediation role of banks between savings and real activity, emphasizing that nonlinearities in financial intermediation can shape growth and stability outcomes [20]. These findings further motivate a systematic PWS modeling framework for banking systems in which macroprudential rules are interpreted as introducing discontinuities and potentially abrupt regime shifts.

Motivated by these insights, the present paper develops an exhaustive analytical study of a one-dimensional piecewise-smooth (PWS) map motivated by the symmetric reduction of a discrete-time dynamical model of a banking duopoly subject to LDR-based reserve requirements. In the reduced framework, the state variable represents the common level of bank loans along the symmetric invariant diagonal, so that its variations capture aggregate credit expansions and contractions within this one-dimensional setting. The switching threshold represents the loan level associated with the lower bound of the LDR corridor. In economic terms, this threshold is determined by the regulatory lower bound on the loan-to-deposit ratio together with the limiting deposit capacity, namely the deposit base available to support lending. When the level of loans is below this threshold, the macroprudential instrument is binding, and banks operate under a tighter reserve regime. When the level of loans is at or above the threshold, the requirement is non-binding. Within this reduced PWS framework, crossings of the threshold correspond to endogenous switches between two policy regimes. In each regime, effective lending incentives summarize lending profitability, adjustment speed, and regulation-induced costs.

Building on the economic interpretation of the proposed PWS model, our contribution is twofold. First, we provide a complete analytical classification of the long-run dynamics of the map, identifying and examining thirteen distinct scenarios. From a mathematical perspective, these scenarios depend on the position and stability properties of the fixed points relative to the map's discontinuity (boundary), as well as on the shape of each branch.

Second, we relate each scenario to the underlying banking framework, showing how different configurations of macroprudential intensity and structural characteristics of the banking sector can sustain a variety of lending dynamics through BCBs. These include abrupt transitions from stable credit equilibria to persistent cycles, the coexistence of multiple attractors, and chaotic fluctuations.

The remainder of the paper is organized as follows. After this Introduction, Section 2 introduces the one-dimensional PWS map studied in the paper and then explains how it can be motivated as the symmetric diagonal reduction of the banking-duopoly framework proposed by Ansori et al. [16]. Section 3, which constitutes the core of the paper, provides a comprehensive analysis of all possible dynamical scenarios, characterizing the long-run behavior of the map and clarifying the economic interpretation of the relevant parameter configurations. Finally, Section 4 concludes and outlines possible extensions of the analysis. All analytical results are supported by numerical simulations performed in MATLAB.

2. The one-dimensional PWS map and its economic motivation

In this Section, we first introduce the one-dimensional piecewise-smooth (PWS) map that constitutes the main object of our analysis. The map is defined as

$$x_{t+1} = \begin{cases} f_1(x_t) = -\eta x_t^2 + \mu_1 x_t, & x_t < \theta \\ f_2(x_t) = -\eta x_t^2 + \mu_2 x_t, & x_t \geq \theta. \end{cases} \tag{1}$$

where $\eta > 0$, $\theta > 0$, and $\mu_1 > \mu_2 > 1$. The discontinuity point θ separates two regimes, while the parameters μ_1 and μ_2 determine the effective growth factors of the two logistic-type branches. Since both branches are topologically related to the logistic map, the local behavior of each branch is well understood; however, the switching mechanism at $x = \theta$ may generate global dynamics that cannot be inferred from the two branches separately.

The restriction $\mu_1 > \mu_2 > 1$ is imposed throughout the paper in order to focus on the parameter region in which the nonzero fixed points of the two branches are positive and hence economically meaningful. This assumption should be understood as an additional restriction defining the class of one-dimensional maps studied here. Consequently, the connection with the underlying planar banking-duopoly model discussed below is meant to provide an economic motivation for the map, rather than a complete description of the full two-dimensional dynamics.

Indeed, the analysis of the invariant diagonal of a two-dimensional dynamical system does not, in general, characterize the genuine planar dynamics of the original model. For this reason, the results obtained in the present paper should be interpreted as describing the dynamics of the reduced one-dimensional PWS framework along the symmetric invariant manifold. The economic interpretations proposed below are therefore intended as interpretations of this reduced framework, and not as exhaustive conclusions on the global dynamics of the full planar system.

The map in Eq. (1) can be motivated from the banking-duopoly framework proposed by Ansori et al. [16]. In that model, banks adjust loan quantities under a Loan-to-Deposit Ratio Reserve Requirement (LDR–RR), which introduces a regime switch whenever the LDR crosses the regulatory lower bound. We recall the main ingredients of that framework in order to clarify the economic origin of the two branches and of the threshold appearing in Eq. (1).

Ansori et al. [16] analyze a banking duopoly model subject to a macroprudential instrument currently adopted in Indonesia, known as the Loan-to-Deposit Ratio Reserve Requirement (LDR-RR). This policy links the required reserves to a target corridor for the loan-to-deposit ratio (LDR) and implements a penalty scheme whenever a bank operates outside the corridor. In particular, when the LDR falls below its lower bound — a situation that may arise either because deposits are unusually high or because loans are unusually low — banks face an additional LDR-based reserve requirement at the central bank, which makes remaining in the low-LDR region costly and creates incentives to return to the corridor by expanding lending (and/or reducing deposits). In our framework we focus on the second channel: we interpret a low LDR as reflecting subdued lending during downturns, while deposits are assumed to converge to their carrying capacity.[1] Under this interpretation, a higher low-LDR reserve requirement (*i.e.*, a stronger disincentive when the LDR is too low) can induce banks to extend more credit, thereby supporting households and firms during periods of economic distress [18,19].

Accordingly, Ansori et al. [16] develop a banking duopoly model grounded in the structure of Indonesian bank balance sheets. For each bank $i = 1, 2$ at time t the balance sheet consists of deposits $D_{i,t}$, equity $E_{i,t}$, reserve requirements $R_{i,t}$ (including the LDR-RR component), loan quantity $L_{i,t}$, and liquid assets $A_{i,t}$. The resulting duopoly framework gives rise to a two-dimensional piecewise-smooth (PWS) map describing the dynamics of loan quantities, which is written as follows:

$$\begin{cases} L_{1,t+1} = \begin{cases} L_{1,t} + \alpha_1 L_{1,t}(a_1 - \Lambda_1 - b_1 L_{2,t} - 2b_1 L_{1,t}), & \frac{L_{1,t}}{D_{1,t}} \geq \delta_{lb} \\ L_{1,t} + \alpha_1 L_{1,t}(a_1 - \Lambda_1 - b_1 L_{2,t} - 2b_1 L_{1,t} + r_{A,1}\gamma_{lb}), & \frac{L_{1,t}}{D_{1,t}} < \delta_{lb} \end{cases} \\ L_{2,t+1} = \begin{cases} L_{2,t} + \alpha_2 L_{2,t}(a_2 - \Lambda_2 - b_2 L_{1,t} - 2b_2 L_{2,t}), & \frac{L_{2,t}}{D_{2,t}} \geq \delta_{lb} \\ L_{2,t} + \alpha_2 L_{2,t}(a_2 - \Lambda_2 - b_2 L_{1,t} - 2b_2 L_{2,t} + r_{A,2}\gamma_{lb}), & \frac{L_{2,t}}{D_{2,t}} < \delta_{lb}, \end{cases} \end{cases} \tag{2}$$

where $a_i, b_i > 0$ are positive constants,[2] δ_{lb} is the lower bound of the LDR, γ_{lb} is the lower disincentive, and α_i represents the speed of adjustment in loan dynamics. Moreover, $\Lambda_i = r_{A,i}(1-\kappa_i) + \kappa_i r_{E,i} + c_{L,i} > 0$ and total operating costs are given by $C_{i,t} = c_{D,i} D_{i,t} + c_{L,i} L_{i,t}$ where $0 < c_{D,i}, c_{L,i} < 1$, and $\kappa_{car} \leq \kappa_i < 1$ (with κ_{car} denoting the minimum percentage in the CAR policy set by the central banks [16,19]), $r_{A,i}$ is the constant rate of return on liquid assets and $r_{E,i}$ is the constant cost of equity.

Ansori et al. [16] provide a detailed analysis of Eq. (2) and introduce the following simplifications. They restrict the analysis to the case in which the deposit $D_{i,t}$ of each bank converges to its carrying capacity K_i. In the symmetric case considered below, the two banks are assumed to have the same limiting deposit capacity, denoted by $K = K_1 = K_2$. Economically, K can be interpreted as the limiting deposit base available to support lending. They further assume: $\alpha_1 = \alpha_2 = \alpha$, $a_1 = a_2 = a$, $b_1 = b_2 = b$, $r_{A,1} = r_{A,2} = r_A$, $r_{E,1} = r_{E,2} = r_E$, $\kappa_1 = \kappa_2 = \kappa$, $c_{L,1} = c_{L,2} = c$, $K_1 = K_2 = K$, $\Lambda_1 = \Lambda_2 = \Lambda$.

Therefore, Eq. (2) becomes

$$\begin{cases} L_{1,t+1} = \begin{cases} L_{1,t} + \alpha L_{1,t}(a - \Lambda - bL_{2,t} - 2bL_{1,t}), & L_{1,t} \geq \delta_{lb} K \\ L_{1,t} + \alpha L_{1,t}(a - \Lambda - bL_{2,t} - 2bL_{1,t} + r_A\gamma_{lb}), & L_{1,t} < \delta_{lb} K \end{cases} \\ L_{2,t+1} = \begin{cases} L_{2,t} + \alpha L_{2,t}(a - \Lambda - bL_{1,t} - 2bL_{2,t}), & L_{2,t} \geq \delta_{lb} K \\ L_{2,t} + \alpha L_{2,t}(a - \Lambda - bL_{1,t} - 2bL_{2,t} + r_A\gamma_{lb}), & L_{2,t} < \delta_{lb} K. \end{cases} \end{cases} \tag{3}$$

It can be shown that the phase space of the system is partitioned into the following four regions:

$$R_1 = \{(L_1, L_2) \in \mathbb{R}^2_+ : L_1 \geq \delta_{lb} K, L_2 \geq \delta_{lb} K\}, \tag{4}$$

$$R_2 = \{(L_1, L_2) \in \mathbb{R}^2_+ : L_1 < \delta_{lb} K, L_2 \geq \delta_{lb} K\}, \tag{5}$$

$$R_3 = \{(L_1, L_2) \in \mathbb{R}^2_+ : L_1 < \delta_{lb} K, L_2 < \delta_{lb} K\}, \tag{6}$$

$$R_4 = \{(L_1, L_2) \in \mathbb{R}^2_+ : L_1 \geq \delta_{lb} K, L_2 < \delta_{lb} K\}. \tag{7}$$

Consequently, the system is a piecewise-defined map composed of four branches, denoted by S_1, S_2, S_3, S_4, depending on whether $(L_1, L_2) \in R_i$, with $i = 1, 2, 3, 4$.

Ansori et al. [16] show that the "diagonal" of the system, obtained by imposing

$$L_{1,t} = L_{2,t},$$

[1] Accordingly, adjustments in the LDR mainly occur through loans, and we focus on how changes in the LDR-based reserve requirement affect lending.

[2] Please see the benchmark model [16] for more details.

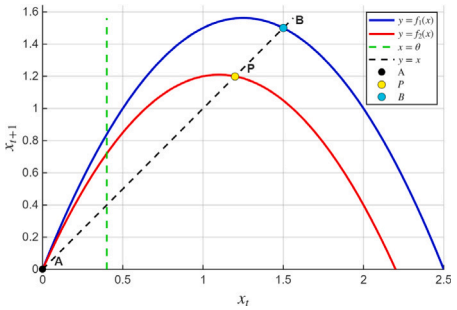

Fig. 1. Parabolas with parameters $\eta = 1, \mu_1 = 2.5, \mu_2 = 2.2, \theta = 0.4$.

is a positively invariant set for Eq. (3). Therefore, we can study the restriction of the system to the main diagonal; the resulting reduced dynamics can be described by the following one-dimensional map:

$$L_{t+1} = \begin{cases} L_t + \alpha L_t(a - \Lambda - 3bL_t), & L_t \geq \delta_{lb}K \\ L_t + \alpha L_t(a - \Lambda - 3bL_t + r_A\gamma_{lb}), & L_t < \delta_{lb}K. \end{cases} \tag{8}$$

For mathematical convenience, Eq. (8) can be rewritten by introducing the following parameters:

$$\begin{aligned} \eta &= 3\alpha b, \\ \mu_1 &= 1 + \alpha(a - \Lambda + r_A\gamma_{lb}), \\ \mu_2 &= 1 + \alpha(a - \Lambda), \\ \theta &= \delta_{lb}K. \end{aligned} \tag{9}$$

with θ acting as the critical threshold that determines the switching between the two regimes of the map.

With this notation, Eq. (8) coincides with the one-dimensional PWS map introduced in Eq. (1). Moreover, we assume $a > \Lambda$, since Ansori et al. [16] show that this condition is essential to ensure the positivity of the equilibria and hence, their economic meaning. Consequently, in our reduced one-dimensional model, $\mu_1 > \mu_2 > 1$.

Since, in Eq. (1), both f_1 and f_2 are topologically conjugate to the logistic map $z' = \mu z(1 - z)$, the local dynamics of each branch are well understood [21,22].

Noticeably, as the parameter θ varies, the map gives rise to thirteen distinct dynamical scenarios.

To make the subsequent scenario analysis self–contained, we first recall some standard results concerning the local dynamics of each smooth branch f_i, $i = 1, 2$, which will be repeatedly used in the analysis of the global behavior of the map.

To determine the fixed points of f_i, we solve

$$f_i(x) = -\eta x^2 + \mu_i x = x, \tag{10}$$

which yields the solutions $x = 0$ and $x = \frac{\mu_i - 1}{\eta}$.

Consequently, the fixed points of Eq. (1) are A, B, and P with $x_A = 0$, $x_B = \frac{\mu_1 - 1}{\eta}$, and $x_P = \frac{\mu_2 - 1}{\eta}$, respectively.

In our framework, a fixed point is said to be real if it lies in the domain of the considered scenario. Therefore, we can observe that since $\mu_1 > \mu_2$, B and P cannot be real at the same time. A statement follows:

Theorem 1. *B and P are stable if and only if $\mu_i \in (1, 3)$, while A is always unstable.*

Proof. For the map $f_i(x) = -\eta x^2 + \mu_i x$ the derivative is $f_i'(x) = -2\eta x + \mu_i$ which, evaluated at the fixed point $x^\star = \frac{\mu_i - 1}{\eta}$, gives $f_i'(x^\star) = 2 - \mu_i$. Finally, $|2 - \mu_i| < 1 \Leftrightarrow \mu_i \in (1, 3)$. □

More specifically, local stability does not depend on the parameter η but only on μ_i, $i = 1, 2$. Indeed, μ_1 determines the local stability of the fixed point B, whereas μ_2 determines the local stability of P. Furthermore, as the parameter μ_i increases, each branch undergoes the classical period-doubling route to chaos up to the critical value $\mu_i = 4$, beyond which trajectories diverge [21].

As for the global behavior, the map in Eq. (1) is composed by two parabolas with downward concavity (since $-\eta < 0$). Depending on the parameter θ, at which the functional form of the dynamics changes, different scenarios may arise. In particular, fixed points may be either admissible or virtual, depending on their location relative to the boundary.

Figs. 1–4 help visualize the following cases:

- if $\theta \in (0, \frac{\mu_2 - 1}{\eta})$, then P is real;
- if $\theta = \frac{\mu_2 - 1}{\eta}$, then a BCB of the fixed point P occurs;
- if $\theta \in (\frac{\mu_2 - 1}{\eta}, \frac{\mu_1 - 1}{\eta})$, then both P and B are virtual;

- if $\theta = \frac{\mu_1 - 1}{\eta}$, then a BCB of the fixed point B occurs;
- if $\theta \in (\frac{\mu_1 - 1}{\eta}, \frac{\mu_2}{\eta})$, then B is real;
- if $\theta \in (\frac{\mu_2}{\eta}, \frac{\mu_1}{\eta})$, then f_2 produces only values of x_{t+1} that are not economically meaningful and hence, this case is not relevant.

Furthermore, we impose $\frac{\mu_1 - 1}{\eta} < \frac{\mu_2}{\eta}$, *i.e.*, $\mu_1 < \mu_2 + 1$, since otherwise f_2 becomes ineffective before the fixed point B is reached, leading to a less rich dynamical structure.

In order to prevent trajectories from becoming negative or diverging (in accordance with the economic interpretation of the model), we study Eq. (1) under the assumptions of the following result:

Theorem 2. *If $\mu_1^2 - 4\mu_2 \leq 0$, then the interval $I = [0, \frac{\mu_2}{\eta}]$ is positively invariant for the map.*

Proof. Since $f_1 > f_2$ and the maximum of f_1 is attained at its vertex $V_1 = (\frac{\mu_1}{2\eta}, \frac{\mu_1^2}{4\eta})$, then the dynamics cannot exceed the intersection of f_2 with the x-axis if $\frac{\mu_1^2}{4\eta} < \frac{\mu_2}{\eta}$. Therefore, trajectories starting in I remain in I, proving positive invariance. □

3. Analysis of the different scenarios

In this Section, we present the thirteen possible scenarios, classified according to which fixed point is admissible and its position along the corresponding branch (in the increasing region of the parabola, at its maximum, or in the decreasing region). The resulting long-run dynamics may vary substantially across scenarios.

To begin with, observe that the fixed point of f_i lies on the increasing side of the parabola if $\mu_i < 2$, coincides with the vertex $V_i(\frac{\mu_i}{2\eta}, \frac{\mu_i^2}{4\eta})$ if $\mu_i = 2$, and lies on the decreasing side if $\mu_i > 2$.

In Figs. 2–4, we depict and label all these scenarios. Consistently with the caveat discussed in Section 2, the following economic interpretations refer to the reduced one-dimensional dynamics along the symmetric invariant manifold, and not to the full planar dynamics of the original banking-duopoly model. From an economic perspective, the classification illustrated in Figs. 2–4 organizes the possible long–run behaviors of the symmetric banking duopoly under an LDR–based reserve requirement. The two fixed points, B and P, represent stationary loan levels under, respectively, the regime in which the macroprudential instrument is binding ($x_t < \theta$, branch f_1) and the regime in which it is non-binding ($x_t \geq \theta$, branch f_2). Whether these fixed points are real or virtual determines whether the corresponding stationary configurations are attainable in the long run or instead remain "latent" benchmarks that influence the dynamics through the shape of the map.

The position of the discontinuity θ, which reflects the chosen LDR threshold δ_{lb}, therefore plays a crucial role. By shifting θ, the regulator effectively moves the boundary between the two policy regimes, potentially triggering abrupt transitions from regions characterized by a unique stable equilibrium to regions exhibiting multiple attractors or purely chaotic dynamics.

A detailed discussion of each scenario follows, organized according to the following structure: cases in which B is real (Section 3.1), cases in which P is real (Section 3.2), cases in which both P and B are virtual (Section 3.3). Subsequently, we examine in detail the scenarios associated with BCBs involving point B (Section 3.4) and point P (Section 3.5).

3.1. Cases in which B is real

We consider the scenarios in which the fixed point B is real, that is, $\theta \in (\frac{\mu_1 - 1}{\eta}, \frac{\mu_2}{\eta})$.

Since similar arguments apply, we present the following three scenarios together.

3.1.1. Scenario 1

In this scenario, B lays in the increasing side of f_1, that is, $\mu_1 < 2$.

Theorem 3. *Under the above assumptions, the interval $J = [0, \theta]$ is attractive.*

Proof. We first prove that J is positively invariant.

Clearly, if $x_t > 0$, then $x_{t+1} > 0$. Then, in order to prove that $x_t < \theta$ implies $x_{t+1} < \theta$, let us consider the interval J as the union of two disjoint intervals $J_1 = [0, \frac{\mu_1 - 1}{\eta}]$ and $J_2 = (\frac{\mu_1 - 1}{\eta}, \theta]$.

Since in the interval J_1 the map f_1 is monotone increasing, it yields that

$$x_t \in J_1 \implies x_{t+1} \leq \max_{J_1} f_1(x_t) = \frac{\mu_1 - 1}{\eta} < \theta. \tag{11}$$

As for the second interval, let us study separately the case $\theta \in (\frac{\mu_1 - 1}{\eta}, \frac{\mu_1}{2\eta}]$ and the case $\theta \in (\frac{\mu_1}{2\eta}, \frac{\mu_2}{\eta})$. In the first case, if $x_t \in J_2$, then $x_{t+1} < \max_{J_2} f_1(x_t) = f_1(\theta) < \theta$. Similarly, in the second case if $x_t \in J_2$, then $x_{t+1} < \max_{J_2} f_1(x_t) = \frac{\mu_1^2}{4\eta} < \frac{\mu_1}{2\eta} < \theta$. Therefore, the interval J is positively invariant.

Next, we prove the attractiveness of J. Let $x_t \in (\theta, \frac{\mu_2}{\eta})$. Since $\theta > \frac{\mu_1 - 1}{\eta}$ and $\mu_1 > \mu_2$, we have

$$\theta > \frac{\mu_2 - 1}{\eta} = x_P.$$

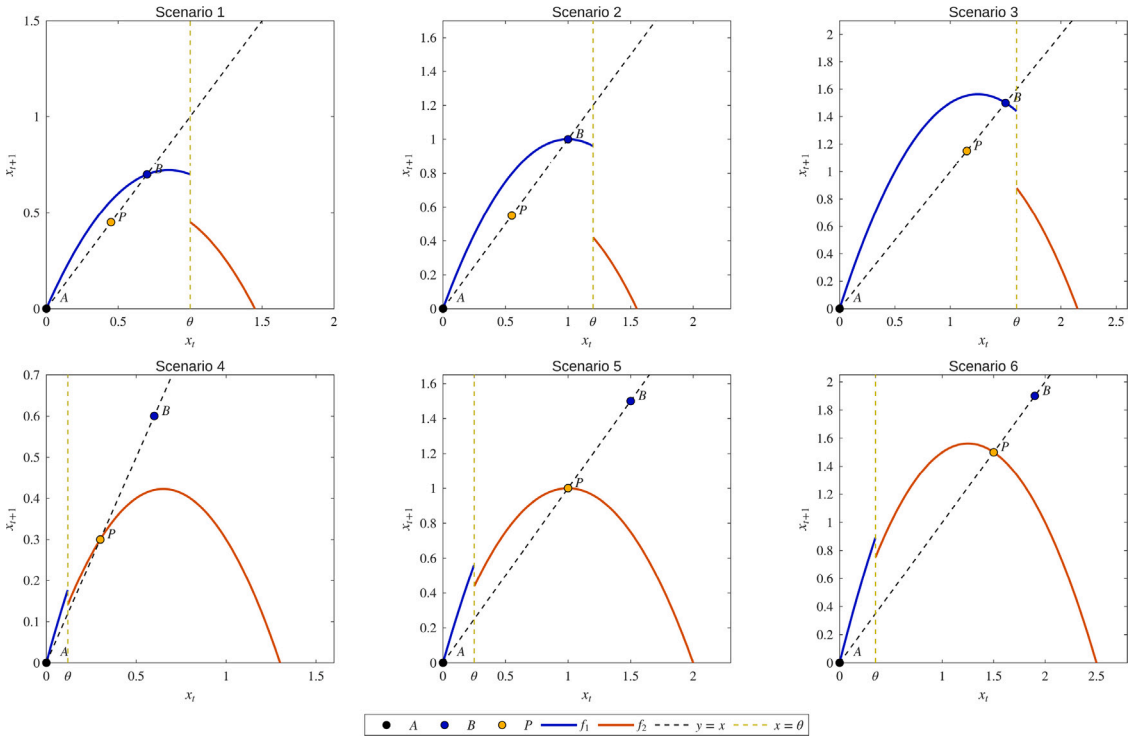

Fig. 2. Scenarios 1–6 with real fixed points. Upper row: Scenarios 1–3, in which B is real. Lower row: Scenarios 4–6, in which P is real. Fixed points: A (black), B (blue), P (yellow). Curves: f_1 (blue), f_2 (red). Dashed lines indicate the bisector $y = x$ (black) and the threshold $x = \theta$ (yellow-green). (For interpretation of the references to color in this figure legend, the reader is referred to the web version of this article.)

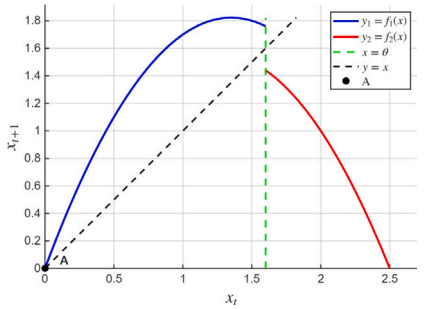

Fig. 3. Scenario 7 with virtual fixed points. Fixed point: A (black). Curves: f_1 (blue), f_2 (red). Dashed lines indicate the bisector $y = x$ (black) and the threshold $x = \theta$ (green). (For interpretation of the references to color in this figure legend, the reader is referred to the web version of this article.)

Therefore, for every $x_t \in (\theta, \frac{\mu_2}{\eta})$,

$$f_2(x_t) - x_t = x_t(\mu_2 - 1 - \eta x_t) < 0.$$

Hence, as long as the orbit remains in $(\theta, \frac{\mu_2}{\eta})$, it is strictly decreasing. Suppose, by contradiction, that the orbit never enters J. Then it converges to a limit $\ell \geq \theta$. By continuity of f_2, this limit must satisfy $\ell = f_2(\ell)$. This is impossible, since the only positive fixed point P of f_2 has abscissa $x_P = \frac{\mu_2 - 1}{\eta} < \theta$. Therefore, the orbit enters J after finitely many iterations. Since J is positively invariant, J is attracting. □

Therefore, there exists a compact attracting set for the map contained in J. Every initial condition generates a bounded trajectory converging to an attractor within J, implying the existence of a global attractor in this interval.

Since $\mu_1 < 2$, the fixed point B is locally asymptotically stable (recall that stability holds for $\mu_1 \in (1, 3)$). Hence B is the global attractor.

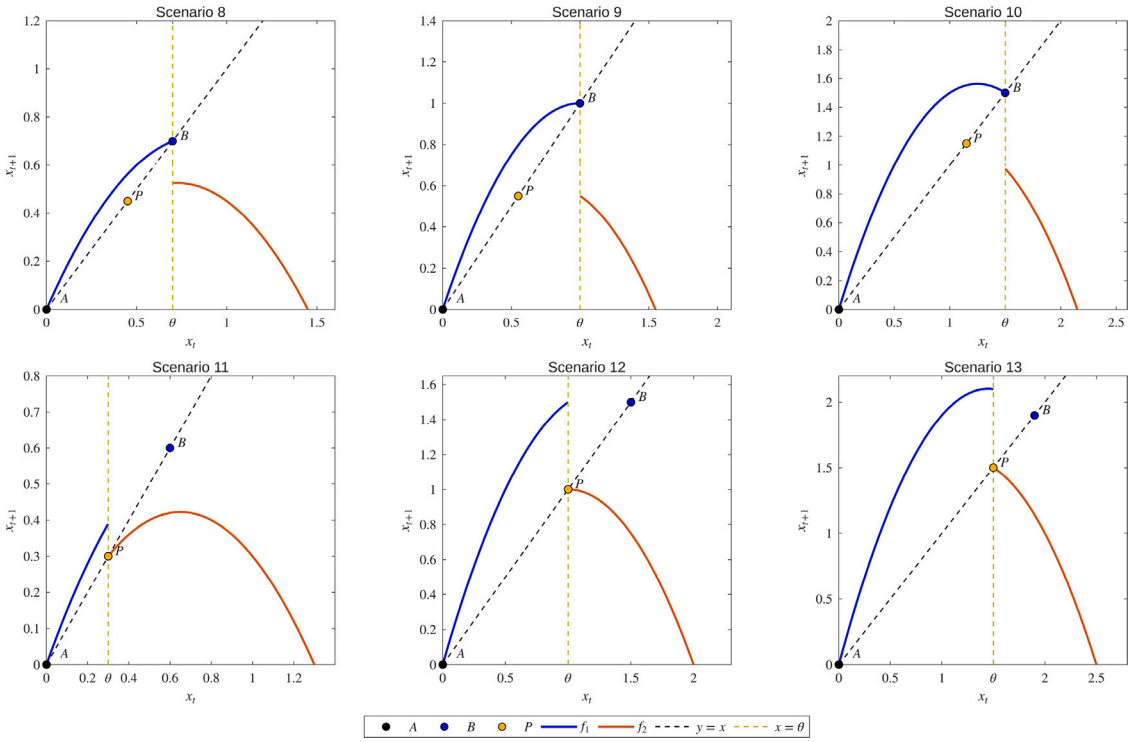

Fig. 4. Upper row: Scenarios 8–10 associated with the border-collision bifurcation of B. Lower row: Scenarios 11–13 associated with the border-collision bifurcation of P. Fixed points: A (black), B (blue), P (yellow). Curves: f_1 (blue), f_2 (red). Dashed lines indicate the bisector $y = x$ (black) and the threshold $x = \theta$ (yellow-green). (For interpretation of the references to color in this figure legend, the reader is referred to the web version of this article.)

3.1.2. Scenario 2

If B lays on the maximum of f_1 and $\mu_1 = 2$, the previous theorem still holds and B is a global attractor for this scenario as well.

3.1.3. Scenario 3

If B lies on the decreasing side of f_1, that is, $\mu_1 > 2$, richer dynamics may arise.

Let us start with the following result:

Theorem 4. *If* $\theta > \frac{\mu_1^2}{4\eta}$, *then Theorem 3 still holds.*

Proof. Under the hypothesis θ is greater than the vertex's ordinate and the proof of Theorem 3 holds. □

Therefore, if we restrict our analysis to $\theta \in (\frac{\mu_1^2}{4\eta}, \frac{\mu_2}{\eta})$, the interval J remains attracting and a global attractor exists inside it.

When $\mu_1 > 2$, increasing the parameter μ_1 from 2 to 4 (where all trajectories diverge), we can observe that the map presents different types of global attractors depending on the value of μ_1.

For instance, chaotic attractors arise for $\mu_1 \approx 3.7$, as shown in Fig. 5.

From an economic point of view, Scenarios 1–3 correspond to configurations in which the stationary loan level associated with the binding LDR–based rule, B, is attainable. In Scenario 1 ($\mu_1 < 2$), the fixed point B lies on the increasing branch of f_1 and is globally attracting. Consequently, regardless of the initial loan level, the symmetric duopoly converges to a unique and stable credit volume below the threshold θ. The macroprudential instrument is permanently active, but its presence stabilizes the system: the higher reserve requirement at low LDR values, combined with gradual adjustment by banks, dampens fluctuations and prevents excessive credit expansion.

In Scenario 2 ($\mu_1 = 2$), the fixed point B coincides with the maximum of f_1. Economically, this case can be interpreted as a critical configuration in which the marginal profitability of additional loans is exactly offset by the marginal cost (including capital and reserve requirements). The equilibrium remains globally attracting, but it sits at the edge between monotone and oscillatory convergence.

Scenario 3 ($\mu_1 > 2$) highlights the potentially destabilizing effects of aggressive credit expansion when the LDR–based instrument is binding. Although B still belongs to the regime $x_t < \theta$, it lies on the decreasing side of f_1 and may lose stability through a standard

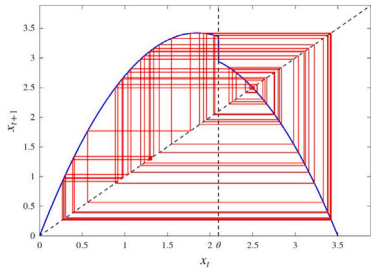

Fig. 5. Cobweb plot of the map when $\eta = 1$, $\mu_1 = 3.7$, $\mu_2 = 3.5$, $\theta = 2.1$, and initial condition $x_0 = 1.3$.

period–doubling bifurcation. As μ_1 increases, the symmetric banking system evolves from a stable fixed point to stable cycles and eventually to chaotic attractors. In economic terms, this reflects a situation in which strong incentives to expand lending (high net profitability or fast adjustment speed α) coexist with a binding macroprudential rule. Rather than smoothing the cycle, the interaction between banks' behavioral rules and regulation may generate endogenous and irregular fluctuations in aggregate loans, making credit conditions highly sensitive to small shocks and parameter changes.

3.2. Cases in which P is real

We now consider the scenarios in which the fixed point P is real, that is, $\theta \in (0, \frac{\mu_2-1}{\eta})$.
First of all, we solve the equation

$$f_2(\tilde{x}) = \theta, \tag{12}$$

whose solutions are $\tilde{x}_{1,2} = f_2^{-1}(\theta) = \frac{\mu_2 \pm \sqrt{\mu_2^2 - 4\eta\theta}}{2\eta}$.

Theorem 5. *If either $\mu_2 \in (1,2]$, or $\mu_2 \in (2,4]$ and $\theta < \frac{4\mu_2^3 - \mu_2^4}{16\eta}$, then the interval $M = [\theta, \tilde{x}_2]$ is positively invariant.*

Proof. We need to prove that if $x \in (\theta, \tilde{x_2})$, then $f_2(x) \in (\theta, \tilde{x_2})$.
On this interval, the minimum of f_2 is $\min\{\theta, f_2(\theta)\}$, while its maximum is $\frac{\mu_2^2}{4\eta}$. We proceed in two steps:

1. $f_2(\theta) > \theta$ if and only if $-\eta\theta^2 + \mu_2\theta > \theta$, which is equivalent to $\theta < \frac{\mu_2-1}{\eta}$.
2. $\frac{\mu_2^2}{4\eta} < \tilde{x_2}$ if and only if $\frac{\mu_2^2}{4\eta} < \frac{\mu_2 + \sqrt{\mu_2^2 - 4\eta\theta}}{2\eta}$. After straightforward algebraic manipulations, the condition becomes $2\sqrt{\mu_2^2 - 4\eta\theta} > \mu_2^2 - 2\mu_2$.

Therefore, if $\mu_2 \in (1,2]$, or if $\mu_2 \in (2,4]$ and $\theta < \frac{4\mu_2^3 - \mu_2^4}{16\eta}$, then the interval M is positively invariant. □

It is worth pointing out the following observations:

- Numerical evidence suggests that when the conditions in the statement of Theorem 5 are fulfilled, the interval M is also attracting;
- the abscissa of the fixed point P belongs to the interval M under the hypotheses of Theorem 5;
- in Scenarios 4 and 5, the hypotheses of Theorem 5 are always satisfied. Hence, there exists a compact set that is positively invariant and (according to the numerical evidence) also attracting. In this case, since the abscissa of P belongs to the interval M, the global attractor coincides with the fixed point P;
- in Scenario 6 under the hypothesis of Theorem 5 the dynamics may exhibit different types of global attractors, as in Scenario 3 (see Fig. 6).

Moreover, in the case $\mu_2 > 2$, let

$$q = \frac{\mu_2^2}{4\eta}$$

be the maximum value of the branch f_2. If $q < \tilde{x}_2$, then the interval whose endpoints are q and $f_2(q)$ is absorbing for the dynamics generated by the right branch f_2. Indeed, after transients, the orbit is confined to the region $x_t \geq \theta$, as long as the maximum of f_2 does not exceed the upper preimage $\tilde{x}_2$ of θ. This provides an additional interpretation of M as a trapping region for the asymptotic dynamics on the right branch.

When P is real, the attainable stationary loan level belongs to the regime $x_t \geq \theta$, where the LDR–based requirement is non-binding and the dynamics is driven by the parameter μ_2. Scenarios 4 and 5 correspond to the case $\mu_2 \in (1,2]$, so that P lies on

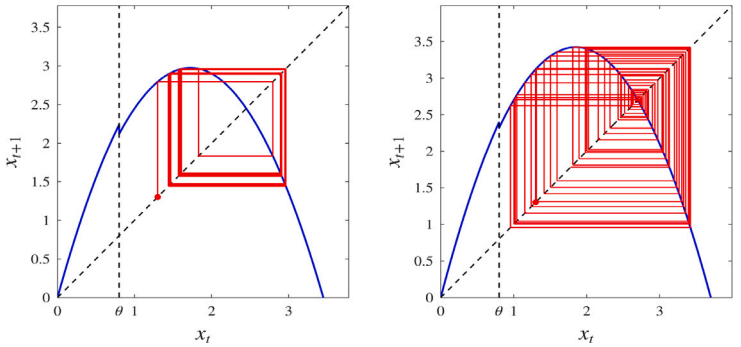

Fig. 6. Cobweb plots of the map. On the left, $\eta = 1$, $\mu_1 = 3.6$, $\mu_2 = 3.45$, $\theta = 0.8$, and initial condition $x_0 = 1.3$, leading to an attracting 4-cycle. On the right, $\eta = 1$, $\mu_1 = 3.8$, $\mu_2 = 3.7$, $\theta = 0.8$, and initial condition $x_0 = 1.3$, leading to nonregular dynamics.

the increasing part of f_2 and is locally (and, according to numerical evidence, globally) stable. Economically, this configuration describes a symmetric duopoly that settles at a relatively high LDR, yet still within the preferred corridor, without triggering corrective macroprudential action. Credit converges to a steady level determined by the structural parameters of the banking sector and remains stable over time.

Scenario 6 exhibits a richer dynamical configuration. As μ_2 increases beyond 2, the fixed point P moves to the decreasing side of f_2 and may lose stability through a sequence of period-doubling bifurcations, leading to higher-period cycles and eventually to chaotic attractors, as illustrated in Fig. 6. This regime corresponds to a weakly regulated credit market in which the intrinsic nonlinearity of banks' adjustment rules is sufficiently strong to generate endogenous credit cycles, even though the LDR threshold θ is not reached in the long run. In such a setting, small variations in structural or regulatory parameters may produce large macroeconomic effects by shifting the system from stable to unstable regions of the parameter space.

3.3. Cases in which both B and P are virtual

If $\theta \in (\frac{\mu_2-1}{\eta}, \frac{\mu_1-1}{\eta})$, then both P and B are virtual and the dynamics may become particularly rich.

3.3.1. Existence of 2-cycles

We first investigate whether there exists a set of parameters for which a 2-cycle arises in this configuration. For this purpose, let $\{x, z\}$ satisfy $f_2(x) = z$ and $f_1(z) = x$. If such values exist, then $\{x, z\}$ is a 2-cycle for Eq. (1).

Substituting z into the second equation yields

$$-\eta^3 x^4 + 2\mu_2\eta^2 x^3 - \eta x^2(\mu_1 + \mu_2^2) + \mu_1\mu_2 x = x. \tag{13}$$

Discarding the trivial solution $x = 0$ and setting $y = \eta x$, we obtain the cubic equation

$$y^3 - 2\mu_2 y^2 + y(\mu_1 + \mu_2^2) + 1 - \mu_1\mu_2 = 0. \tag{14}$$

Standard calculus arguments (analysis of the limits as $y \to \pm\infty$ and the first derivative y') yield the following result.

Theorem 6. *If $\mu_2^2 - 3\mu_1 \le 0$, then there exists a unique 2-cycle for the map in Eq. (1);*
if $\mu_2^2 - 3\mu_1 > 0$, then there exist m distinct 2-cycles for the map in Eq. (1), with $m = 1, 2, 3$.

Proof. Let $g(y) = y^3 - 2\mu_2 y^2 + y(\mu_1 + \mu_2^2) + 1 - \mu_1\mu_2$. From smooth function theory, if $g'(y) > 0 \quad \forall y$ then g is increasing monotonically. Since $g(0) = 1 - \mu_1\mu_2 < 0$, the monotony of g implies that there exists a unique positive intersection with the horizontal axis, *i.e.*, there exists a unique 2-cycle for the map.

Hence, we compute $g'(y) = 3y^2 - 4\mu_2 y + \mu_1 + \mu_2^2$ and solve $g'(y) = 0$, whose solutions are $y_{1,2} = \frac{2\mu_2 \pm \sqrt{\mu_2^2 - 3\mu_1}}{3}$.

Therefore, if $\mu_2^2 - 3\mu_1 \le 0$, then $g'(y) \ge 0$ and the function is monotone non decreasing (unique 2-cycle). On the other hand, if $\mu_2^2 - 3\mu_1 > 0$, then $g'(y) > 0$ in the intervals $\left(-\infty, \frac{2\mu_2 - \sqrt{\mu_2^2 - 3\mu_1}}{3}\right) \quad \vee \quad \left(\frac{2\mu_2 + \sqrt{\mu_2^2 - 3\mu_1}}{3}, +\infty\right)$, meaning that $g(y)$ can have between one and three intersections with the horizontal axis. □

The previous Theorem ensures the existence of at least one 2-cycle $\{x, z\}$ for the map in the present scenario. Its local stability can be studied by solving the inequality $| f_2'(x) f_1'(z) | < 1$, which corresponds to the standard stability criterion for a periodic orbit of period two.

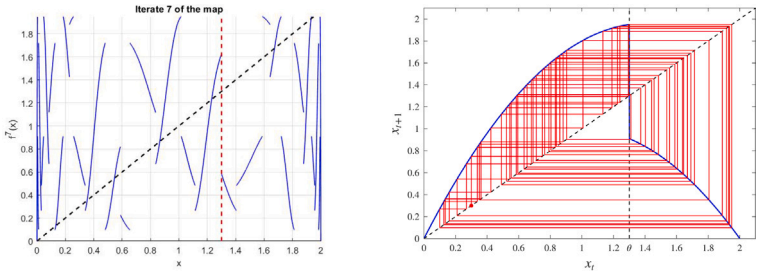

Fig. 7. On the left, it is depicted the seventh iterate of the map with parameters $\eta = 1$, $\mu_1 = 2.8$, $\mu_2 = 2$, $\theta = 1.3$. On the right, the corresponding cobweb plot with initial condition $x_0 = 0.3$.

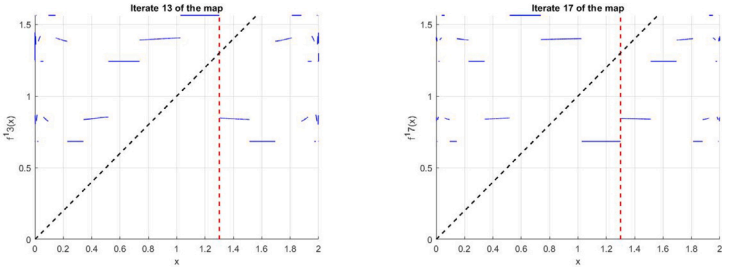

Fig. 8. On the left, it is depicted the thirteenth iterate of the map with parameters $\eta = 1$, $\mu_1 = 2.5$, $\mu_2 = 2$, $\theta = 1.3$. On the right, the seventeenth iterate with the same parameters.

3.3.2. Higher-period cycles and complex dynamics

Numerical investigations performed in MATLAB reveal that this scenario exhibits additional complex dynamical features.

In particular, periodic points can be investigated by considering the iterates of the map in Eq. (1) and by checking whether the graph of the kth iterate intersects the bisector of the first and third quadrant. It is important to stress that an intersection between the graph of f^k and the bisector identifies a periodic point whose primitive period divides k, but it does not necessarily correspond to a cycle of primitive period k. Therefore, the numerical evidence reported below should be interpreted with this distinction in mind.

For instance, setting the parameters to $\eta = 1$, $\mu_1 = 2.8$, $\mu_2 = 2$ and $\theta = 1.3$, we observe that the iterates of the map become increasingly intricate as k grows. Fig. 7 displays the seventh iterate of the map together with its intersections with the bisector, as well as the corresponding cobweb plot for the same parameter values and initial condition $x_0 = 0.3$. These computations suggest a rich periodic structure, although they do not by themselves imply the coexistence of attracting cycles, since the periodic points detected through the iterates may be unstable.

Interestingly, numerical simulations with small changes in the previous parameters suggest different patterns.

For example, if we set $\mu_1 = 2.5$ while keeping the other parameters unchanged, numerical evidence indicates that no periodic points of period k are detected for some prime values $k \geq 5$. For instance, as illustrated in Fig. 8, the thirteenth and seventeenth iterates of the map do not intersect the bisector $y = x$, suggesting the absence of detected 13- and 17-cycles for this parameter configuration.

For this parameter configuration, the only attracting cycles detected numerically are a 2-cycle and a 3-cycle, as illustrated in Fig. 9. More precisely, Fig. 9 shows that different initial conditions may converge to different attracting cycles. The basin of attraction of the 2-cycle consists of the interval $[\theta, f_{2,+}^{-1}(f_{1,-}^{-1}(\theta))]$ and all its preimages, where $f_{1,-}^{-1}$ corresponds to the inverse branch of f_1 with $x < \theta$ and $f_{2,+}^{-1}$ corresponds to the inverse branch of f_2 with $x \geq \theta$. Hence, this basin is generally disconnected and consists of a countable number of components. The basin of the 3-cycle is the complement of the basin of the 2-cycle.

Moreover, if we set $\eta = 1$, $\mu_1 = 2.7$, $\mu_2 = 2$, $\theta = 1.1$, numerical evidence still indicates that no periodic points of period k are detected for some prime values $k \geq 5$. Nevertheless, if we set $x_0 = 0.3$, the map exhibits a stable 4-cycle, as shown in Fig. 10.

3.3.3. Additional numerical simulations

Finally, it is interesting to visualize some 2−dimensional bifurcation diagrams obtained by varying the parameters μ_1 and μ_2. Fig. 11 illustrates the heterogeneity of the dynamical behavior exhibited by the map under different parameter configurations.

In the parameter windows displayed in Fig. 11, the dashed horizontal line marks the border-collision condition $\mu_2 = 1 + \eta\theta$ for the fixed point P. Since $\mu_1 > 1 + \eta\theta$ throughout the two panels, the fixed point B is virtual in the displayed ranges. Hence, above the dashed line P is real, whereas below it both P and B are virtual. The latter case is particularly interesting from a macroprudential perspective. In this configuration, the two stationary loan levels associated with the binding and non–binding regimes exist as

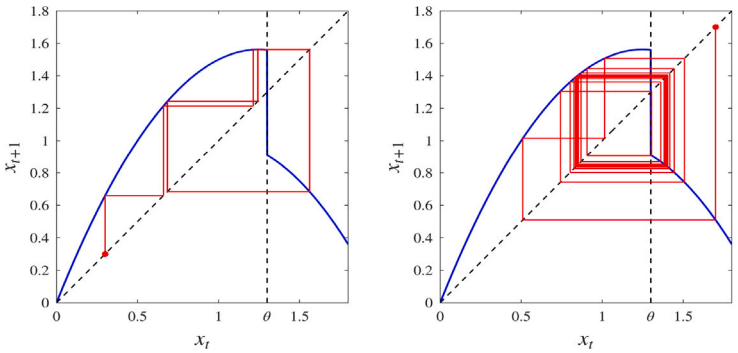

Fig. 9. Cobweb plots of the map when $\eta = 1$, $\mu_1 = 2.5$, $\mu_2 = 2$, and $\theta = 1.3$. On the left, the initial condition is $x_0 = 0.3$. On the right, the initial condition is $x_0 = 1.7$.

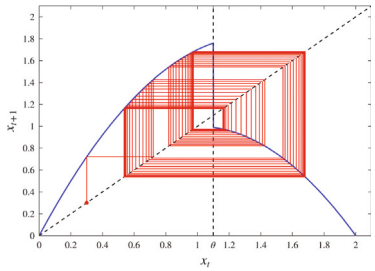

Fig. 10. Cobweb plot of the map when $\eta = 1$, $\mu_1 = 2.7$, $\mu_2 = 2$, $\theta = 1.1$, and initial condition $x_0 = 0.3$.

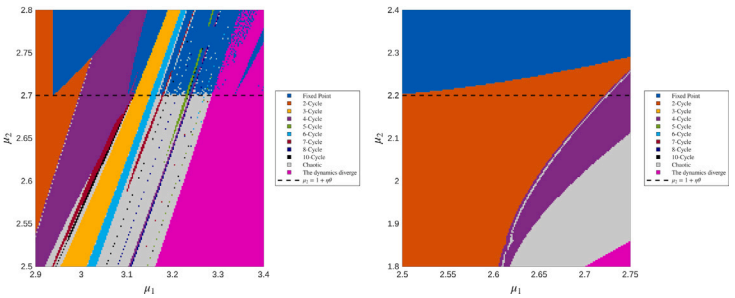

Fig. 11. L.h.s.: the 2-dimensional bifurcation diagram with parameters $\eta = 1$, $\mu_1 \in (2.9, 3.4)$, $\mu_2 \in (2.5, 2.8)$, $\theta = 1.7$ and initial condition $x_0 = 0.3$. R.h.s.: the bifurcation diagram with parameters $\eta = 1$, $\mu_1 \in (2.5, 2.75)$, $\mu_2 \in (1.8, 2.4)$, $\theta = 1.2$ and initial condition $x_0 = 0.3$. The dashed horizontal line marks the border-collision condition $\mu_2 = 1 + \eta\theta$ for the fixed point P.

algebraic solutions of Eq. (1), yet they lie on the "wrong" side of the discontinuity, so that the dynamics cannot converge to either of them. Thus, the dynamics of the banking system may alternate between the two regimes, repeatedly crossing the LDR threshold θ. The emergence of 2–cycles and higher–period cycles in this setting corresponds to persistent, deterministic oscillations of the aggregate LDR around the corridor: in some periods the rule is binding and banks face higher reserve requirements, while in others it is slack and credit expands under the non–binding regime.

The numerically observed coexistence of attracting cycles of different periods, documented in Fig. 9, can be interpreted as a form of endogenous "stop-and-go" credit dynamics. Even in the absence of external shocks, the interaction between the discontinuity at θ and the nonlinear loan-adjustment mechanism generates alternating phases of credit expansion and contraction, accompanied by abrupt switches in the binding status of the macroprudential rule.

For regulators, this suggests that placing the LDR threshold between the two natural fixed points of the system may unintentionally create highly complex and path–dependent dynamics, where long–run outcomes depend sensitively on the initial conditions and on small parameter variations.

3.4. BCB of point B

In this Section, we would like to consider the critical case $\theta = \frac{\mu_1 - 1}{\eta}$ at which the fixed point B collides with the discontinuity. This parameter configuration gives rise to a BCB involving point B.

3.4.1. Scenarios 8, 9 and 10

Unlike Scenario 1, at the critical value

$$\theta = x_B = \frac{\mu_1 - 1}{\eta},$$

the fixed point B collides with the discontinuity. Since the branch f_1 is selected only for $x < \theta$, while the branch f_2 is selected for $x \geq \theta$, the point B is no longer admissible at the collision. When referring to the dynamics after the collision, we mean the parameter configuration in which B has become virtual after crossing the border. In this case, trajectories cannot converge to the former fixed point B. The following result identifies the relevant interval controlling the local dynamics near the border.

Theorem 7. *Assume $\theta = \frac{\mu_1 - 1}{\eta}$, $\mu_2 < \mu_1 < \mu_2 + 1$, and $\mu_1 \leq 2$. Then the interval*

$$J_B = [f_2(\theta), f_1(\theta)] = [f_2(\theta), \theta]$$

is positively invariant and locally absorbing.

Proof. At the BCB, the fixed point B collides with the discontinuity, and hence

$$f_1(\theta) = \theta.$$

Moreover,

$$f_2(\theta) = -\eta\theta^2 + \mu_2\theta = \theta(\mu_2 - \mu_1 + 1).$$

Since $\mu_2 < \mu_1 < \mu_2 + 1$, we have $0 < \mu_1 - \mu_2 < 1$, and therefore

$$0 < \mu_2 - \mu_1 + 1 < 1.$$

It follows that

$$0 < f_2(\theta) < \theta.$$

We first prove positive invariance. Let $x \in [f_2(\theta), \theta)$. Since $x < \theta$, the active branch is f_1. Moreover, $\mu_1 \leq 2$ implies that f_1 is increasing on $[0, \theta]$, and therefore

$$f_1(x) \leq f_1(\theta) = \theta.$$

On the other hand,

$$f_1(x) - x = x(\mu_1 - 1 - \eta x) = \eta x(\theta - x) \geq 0,$$

so that $f_1(x) \geq x \geq f_2(\theta)$. Thus $f_1(x) \in [f_2(\theta), \theta]$. If $x = \theta$, the definition of the map gives $f(\theta) = f_2(\theta)$. Therefore, J_B is positively invariant.

Finally, by continuity of f_2, there exists $\epsilon > 0$ such that $f_2(x) \in (0, \theta)$ for every $x \in [\theta, \theta + \epsilon)$. Taking ϵ sufficiently small also ensures that $(\theta - \epsilon, \theta] \subset J_B$. Hence, every point starting sufficiently close to the border either already belongs to J_B or is mapped into $(0, \theta)$. While the orbit remains in $(0, \theta)$, the active branch is f_1 and

$$f_1(x) - x = \eta x(\theta - x) > 0.$$

Hence the iterates increase toward θ and enter J_B after finitely many iterations. This proves that J_B is locally absorbing. □

The local dynamics around the border is shown in Fig. 12.

From an economic perspective, the BCB of B, occurring at $\theta = (\mu_1 - 1)/\eta$, represents a critical configuration in which the stationary loan level under the binding regime collides with the regulatory threshold. Prior to the bifurcation, in Scenarios 1–3, the symmetric banking system may converge to B or to other attractors entirely contained in the region $x_t < \theta$. At the bifurcation, however, the equilibrium reaches the boundary and becomes virtual: the system can no longer settle at the loan level that would simultaneously satisfy banks' optimality conditions and the LDR constraint.

Scenarios 8 and 9 (with $\mu_1 \leq 2$) show that, when the fixed point B disappears, the local dynamics near the border is confined by the positively invariant and locally absorbing interval $J_B = [f_2(\theta), \theta]$. This interval should not be interpreted as an arbitrarily small neighborhood of the boundary, since its width depends on the parameter values. Economically, confinement in this interval means that trajectories may switch between the two branches of the map, corresponding to alternation between the binding and non-binding LDR regimes. For parameter values corresponding to Scenario 10 ($\mu_1 > 2$), the same mechanism can lead to period–doubling cascades and chaos, implying a highly irregular pattern of credit expansions and contractions driven solely by the interaction between banks' behavior and the discontinuity induced by regulation.

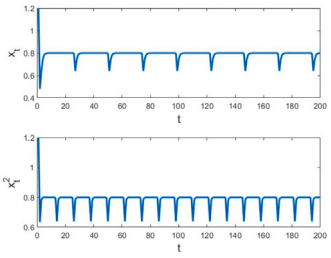

Fig. 12. Trajectories of the map (above) and its second iterate (below) with parameters $\eta = 1, \mu_1 = 1.8, \mu_2 = 1.6, \theta = 0.8$ and initial condition $x_0 = 1.2$.

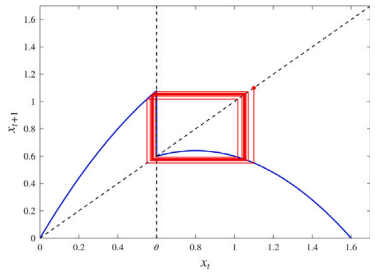

Fig. 13. Cobweb plot of the map when $\eta = 1$, $\mu_1 = 2.4$, $\mu_2 = 1.6$, $\theta = 0.6$, and initial condition $x_0 = 1.1$. The trajectory converges to a stable 2-cycle located outside L.

3.5. BCB of point P

If $\theta = \frac{\mu_2 - 1}{\eta}$, the fixed point P collides with the boundary and a BCB occurs.

3.5.1. Scenario 11

Building on the results obtained in Scenario 4, let $\bar{x} = f_2^{-1}(\theta) = \frac{1}{\eta}$. The following result holds.

Theorem 8. *If $\mu_2 < 2$, then the interval $L = [\theta, \bar{x}]$ is positively invariant.*

Proof. We prove that if $x \in [\theta, \bar{x}]$, then $f_2(x) \in [\theta, \bar{x}]$. On this interval, the minimum of f_2 equals θ, while the maximum is $\frac{\mu_2^2}{4\eta}$. Then, the proof is analogous to that of Theorem 5. □

However, the counterexample reported in Fig. 13 shows that L is not globally attracting. For a specific parameter configuration, the map exhibits a stable 2-cycle located outside L, demonstrating that positive invariance does not imply global attractivity in this case.

Therefore, trajectories starting in L remain in L and converge to P, since we are under the assumption that the fixed point is locally stable. However, this does not imply that L is globally attracting. More precisely, the basin of attraction of P consists of L together with all its preimages. For the parameter configuration reported in Fig. 13, the stable 2-cycle lies outside L, and its basin of attraction is the complement of the basin of P. Consequently, both basins are generally disconnected and consist of a countable number of components.

3.5.2. Scenario 12

In this case, the fixed point P coincides with the maximum of f_2 and therefore cannot be attracting. Indeed, if a trajectory approaches P from the right, the next iterate is governed by f_1; if it approaches P from the left, the orbit reaches the region where f_1 applies within at most two iterations.

Furthermore, since in this scenario $\mu_2 = 2$ and $\theta = \frac{\mu_2 - 1}{\eta} = \frac{1}{\eta}$, in order to guarantee the positive invariance of the interval I, Theorem 2 implies that the parameter μ_1 must satisfy $\mu_1 \in (2, 2\sqrt{2}]$. Building on this restriction, we perform numerical simulations with parameters $\eta = 1, \mu_2 = 2, \theta = 1, x_0 = 0.3$ and changing $\mu_1 \in [2.1, 2\sqrt{2}]$.

In Fig. 14 we observe that the map may exhibit attracting cycles of different periods as well as complex dynamics.

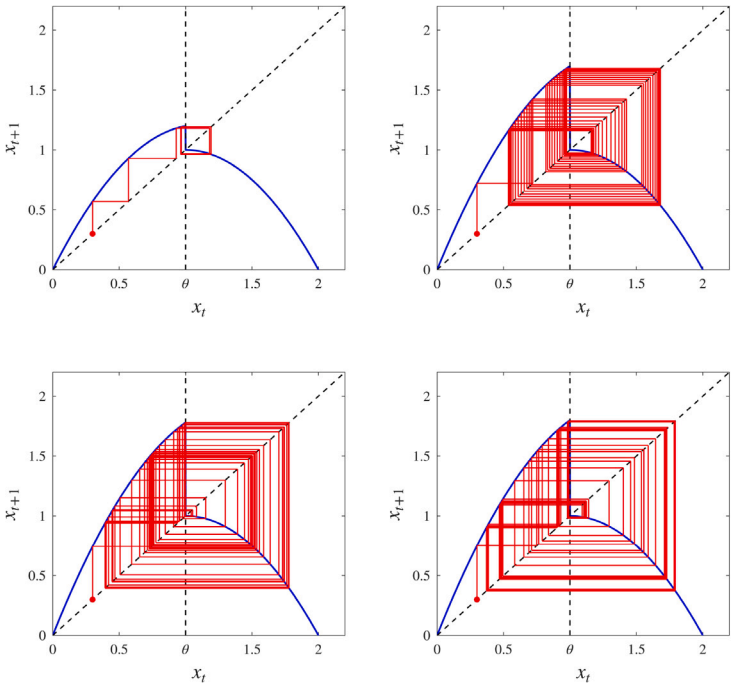

Fig. 14. Cobweb plots of the map with parameters $\eta = 1$, $\mu_2 = 2$, $\theta = 1$, and initial condition $x_0 = 0.3$. Top left: $\mu_1 = 2.2$, attracting 2-cycle. Top right: $\mu_1 = 2.7$, attracting 4-cycle. Bottom left: $\mu_1 = 2.78$, attracting 7-cycle. Bottom right: $\mu_1 = 2.8$, nonregular dynamics.

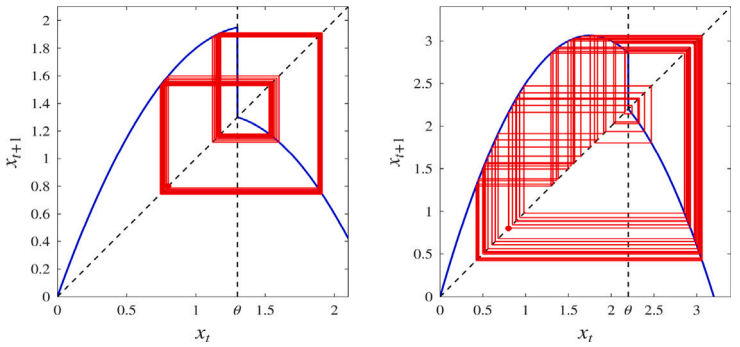

Fig. 15. Cobweb plots of the map. On the left, $\eta = 1$, $\mu_1 = 2.8$, $\mu_2 = 2.3$, $\theta = 1.3$, and initial condition $x_0 = 0.8$, leading to an attracting 4-cycle. On the right, $\eta = 1$, $\mu_1 = 3.5$, $\mu_2 = 3.2$, $\theta = 2.2$, and initial condition $x_0 = 0.8$, leading to nonregular dynamics.

3.5.3. Scenario 13

In this final scenario, although P does not coincide with the maximum point of f_2, it can again be excluded as a potential attractor. Indeed, at the BCB one has $\theta = x_P = \frac{\mu_2 - 1}{\eta}$ and hence, $f_2(\theta) = \theta$. However, the map is discontinuous at θ. Since $\mu_1 > \mu_2$, the left-hand limit satisfies $\lim_{x \to \theta^-} f(x) = f_1(\theta) = \theta + (\mu_1 - \mu_2)\theta > \theta$. Moreover, since in Scenario 13 one has $\mu_2 > 2$, points $x > \theta$ sufficiently close to θ are mapped below the threshold, because $f_2(x) - \theta = (2 - \mu_2)(x - \theta) - \eta(x - \theta)^2 < 0$. The subsequent iterate is therefore governed by f_1 and is moved away from a sufficiently small neighborhood of P. Thus, P is not an attracting fixed point in Scenario 13.

Numerical simulations performed in MATLAB show that, in this configuration, the map may exhibit cycles of different periods as well as complex dynamics, as illustrated in Fig. 15.

The BCB of P at $\theta = (\mu_2 - 1)/\eta$ admits a complementary economic interpretation. In this case, the stationary loan level associated with the non–binding regime collides with the LDR threshold. Prior to the bifurcation, in Scenarios 4–6, the system may converge to P within the region $x_t \geq \theta$. At the bifurcation point, this equilibrium lies exactly on the boundary; beyond it, the fixed point becomes virtual and cannot be attained by the dynamics.

Scenario 11 ($\mu_2 < 2$) shows that, even when P is locally stable and the interval L is positively invariant, additional attractors – such as stable 2-cycles – may coexist outside L. Economically, this implies that the banking system may either converge to a high–LDR stationary configuration with a non-binding macroprudential rule or exhibit persistent credit cycles that repeatedly approach and move away from the regulatory threshold. The realized outcome depends on initial conditions and on the past trajectory of the system, highlighting path dependence.

Finally, in Scenarios 12 and 13 ($\mu_2 \geq 2$), the system may display higher-period cycles and chaotic attractors. In this regime, the credit market becomes intrinsically unstable: the macroprudential instrument is unable either to anchor the system at a stable high–LDR equilibrium or to prevent irregular oscillations. As a result, the long–run behavior of loans becomes highly erratic and difficult to forecast.

4. Conclusions

In this paper, we have characterized the dynamics of the one-dimensional PWS map defined in Eq. (1), which is motivated by the symmetric diagonal reduction of a banking-duopoly framework subject to an LDR-based reserve requirement. The economic interpretation of the results has been developed within this reduced one-dimensional setting. We identified thirteen qualitatively distinct scenarios arising from different parameter configurations and analyzed their associated long-run behaviors. Particular attention was devoted to the emergence of complex dynamics, including multistability and higher-period cycles, combining analytical results with numerical evidence and thereby addressing an existing gap in the literature. We specifically focused on the occurrence of BCBs of the fixed points owned by the map, and the particular case where they are virtual, which is interesting for recent research.

From an economic perspective, the thirteen scenarios provide a complete taxonomy of the possible long-run credit outcomes generated by the interaction between boundedly rational loan adjustment and the LDR-based reserve requirement. The parameters μ_1 and μ_2 summarize the effective incentives to expand credit under the binding and non-binding regimes, respectively, while the threshold $\theta = \delta_{lb}K$ determines the switching point between the two policy environments. Our analysis shows how alternative regulatory designs and structural features of the banking sector translate into qualitatively different aggregate lending regimes.

The role of the fixed points B and P is central for policy implications. When B is admissible (Scenarios 1–3), the binding regime becomes the relevant long-run benchmark: for moderate values of μ_1, the economy converges to a stable low-LDR equilibrium with a persistently active macroprudential instrument. However, as μ_1 increases, this regime may lose stability through period-doubling bifurcations, generating persistent cycles or chaotic credit dynamics. Symmetrically, when P is admissible (Scenarios 4–6), the steady state lies in the non-binding regime, and credit stabilizes at a high-LDR level within the corridor unless strong nonlinear adjustment effects (large μ_2) induce endogenous oscillations.

The most delicate configuration from a policy standpoint arises when both fixed points are virtual. In this case, the system cannot converge to either stationary loan level and may alternate across the regulatory threshold, producing coexistence of attractors, deterministic credit cycles of different periods, and chaotic fluctuations. Economically, this corresponds to an endogenous "stop-and-go" credit dynamics driven purely by regime switching. Small variations in the LDR threshold may therefore induce large and abrupt changes in lending behavior, so that positioning θ between the two natural stationary values may inadvertently amplify instability rather than dampen it.

The two BCBs identified in this study also admit a clear macroprudential interpretation. The collision of B with the threshold ($\theta = (\mu_1 - 1)/\eta$) eliminates a binding-regime equilibrium and may trigger oscillatory or chaotic dynamics even when B is locally stable. Similarly, the collision of P ($\theta = (\mu_2 - 1)/\eta$) removes the attainable non-binding equilibrium. In both cases, abrupt regime shifts in lending arise endogenously as a direct consequence of corridor-type rules, confirming and extending the evidence obtained in the underlying duopoly model [16].

Several extensions may further enrich the analysis. Allowing for asymmetric banks would generate a genuinely two-dimensional PWS system, where diagonal and off-diagonal dynamics interact. Introducing stochastic disturbances or expectation feedbacks would permit a comparison between endogenous nonlinear fluctuations and exogenous volatility. Finally, alternative macroprudential designs – such as asymmetric penalties or time-varying thresholds – could be evaluated within the same framework to assess their effectiveness in enlarging the parameter region associated with stable credit equilibria.

CRediT authorship contribution statement

Serena Brianzoni: Writing – review & editing, Writing – original draft, Visualization, Supervision, Investigation, Formal analysis, Conceptualization. **Giovanni Campisi:** Writing – review & editing, Writing – original draft, Visualization, Software, Conceptualization. **Alessio Frati:** Writing – review & editing, Writing – original draft, Software, Investigation, Formal analysis. **Carlo Lucheroni:** Writing – review & editing, Writing – original draft, Visualization, Supervision, Conceptualization.

Funding

Open access funding provided by Università Politecnica delle Marche within the CRUI-CARE Agreement.

References

[1] D. Radi, F. Lamantia, G.I. Bischi, Benefits and perils of integrated data systems in managing sustainable fishing quotas, Environ. Resour. Econ. 88 (11) (2025) 2845–2883.
[2] H.E. Nusse, E. Ott, J.A. Yorke, Border-collision bifurcations: An explanation for observed bifurcation phenomena, Phys. Rev. E 49 (2) (1994) 1073.
[3] S. Foale, S.R. Bishop, Bifurcations in impact oscillations, Nonlinear Dynam. 6 (3) (1994) 285–299.
[4] T. Puu, I. Sushko, Oligopoly Dynamics, Models and Tools, Springer Verlag, 2002.
[5] T. Puu, I. Sushko, Business Cycle Dynamics, Models and Tools, Springer Verlag, 2006.
[6] S. Brianzoni, G. Campisi, A. Colasante, Nonlinear banking duopoly model with capital regulation: The case of Italy, Chaos Solitons Fractals 160 (2022) 112209.
[7] S. Brianzoni, G. Campisi, Dynamical analysis of a banking duopoly model with capital regulation and asymmetrical costs, Discrete Contin. Dyn. Syst. Ser. B 26 (11) (2021).
[8] S. Brianzoni, E. Michetti, I. Sushko, Border collision bifurcations of superstable cycles in a one-dimensional piecewise smooth map, Math. Comput. Simulation 81 (1) (2010) 52–61.
[9] L. Fanti, The dynamics of a banking duopoly with capital regulations, Econ. Model. 37 (2014) 340–349.
[10] G.I. Bischi, C. Chiarella, I. Sushko, Global Analysis of Dynamic Models in Economics and Finance: Essays in Honour of Laura Gardini, Springer Science & Business Media, 2012.
[11] L. Gardini, F. Tramontana, F. Westerhoff, Heterogeneous speculators and asset price dynamics: Further results from a one-dimensional discontinuous piecewise-linear map, Comput. Econ. 38 (2011) 329–347.
[12] L. Gardini, F. Tramontana, Border collision bifurcations in 1D PWL map with one discontinuity and negative jump. Use of the first return map, Int. J. Bifurc. Chaos 20 (11) (2010) 3529–3547.
[13] L. Gardini, F. Tramontana, I. Sushko, Border collision bifurcations in one-dimensional linear-hyperbolic maps, Math. Comput. Simulation 81 (4) (2010) 899–914.
[14] V. Avrutin, M. Schanz, L. Gardini, Calculation of bifurcation curves by map replacement, Int. J. Bifurc. Chaos 20 (10) (2010) 3105–3135.
[15] I. Sushko, L. Gardini, Degenerate bifurcations and border collisions in piecewise smooth 1D and 2D maps, Int. J. Bifurc. Chaos 20 (07) (2010) 2045–2070.
[16] M.F. Ansori, S. Brianzoni, G. Campisi, Bifurcations and complex dynamics in a banking duopoly model with macroprudential policy, Phys. A 641 (2024) 129730.
[17] A. Bacchiocchi, G.I. Bischi, G. Giombini, Non-performing loans, expectations and banking stability: A dynamic model, Chaos Solitons Fractals 157 (2022) 111906.
[18] D.M. Satria, C.A. Harun, A.A. Taruna, The macro-prudential aspects of loan-to-deposit-ratio-linked reserve requirement, Appl. Econ. 48 (1) (2016) 24–34.
[19] M.F. Ansori, I. Gunadi, N. Sumarti, K.A. Sidarto, Analyzing a macroprudential instrument during the COVID-19 pandemic using border collision bifurcation, Rev. Electrón. Comun. Trab. ASEPUMA 22 (2) (2021) 91–103.
[20] S. Brianzoni, G. Campisi, A. Palestrini, Effects of financial intermediation on real variables: a discrete-time dynamical framework: S. Brianzoni et al., Decis. Econ. Finance 49 (1) (2026) 689–707.
[21] R. May, Simple mathematical models with very complicated dynamics, Nature 261 (1976).
[22] A. Medio, M. Lines, Nonlinear Dynamics, A Primer, Cambridge University Press, 2003.